RESEARCH PAPER

Simultaneous electroanalytical sensing of dopamine and epinephrine using TiO$_2$/reduced graphene oxide nanocomposite modified glassy carbon electrode

Khadijeh Ghanbari*, Fahime Ghorbani, Sepide Bonyadi

Department of Chemistry, Faculty of Physics and Chemistry, Alzahra University, Tehran, Iran

ARTICLE INFO

ABSTRACT

This work introduces a novel electrochemical sensor for simultaneous determination of dopamine (DA) and epinephrine (EP) by modifying a glassy carbon electrode (GCE) with reduced graphene oxide (RGO) and titanium dioxide (TiO2) nanoparticles. The RGO/TiO2 nanocomposite characterization was investigated by using field emission scanning electron microscopy (FE-SEM), elemental mapping, Fourier-transform infrared spectroscopy (FTIR), Raman spectroscopy, X-Ray diffraction analysis (XRD), and X-ray photoelectron spectroscopy (XPS). Cyclic voltammetry (CV) and differential pulse voltammetry (DPV) methods were used for electrochemical measurements. This study showed that the resultant RGO/TiO$_2$ modified GCE is highly sensitive and selective for the simultaneous determination of DA and EP, and provided two linear responses rangeing from 5-180 and 180-1000 μM with a detection limit of 1.3 μM for DA and two linear responses ranging from 5-20 and 20-1000 μM with a detection limit of 1.4 μM for EP. In addition, the electrochemical oxidation of DA and EP was well recovered in pharmaceutical formulations.

INTRODUCTION

The neurotransmitters dopamine (DA), norepinephrine (NE), and epinephrine (EP), belonging to the class of catecholamines, play essential roles in the central nervous system [1]. Given their crucial roles in mammals, they are of significant importance. Catecholamines, which are released into the blood during the body's stress response, are generated in the adrenal glands, brainstem, and the brain. Functioning as hormones, they are broken down after only a few minutes [2], and then excreted in the urine [3]. Thus, the concentration of catecholamines must be monitored in biological fluids for neurochemical and medical purposes since they can signal the emergence of different diseases such as Parkinson's disease, HIV, schizophrenia, tumors, diabetes, and cirrhosis [4-6].

Different methods including chromatography [7, 8], mass spectroscopy [9, 10], capillary electrophoresis [11], and electrochemical approaches [12, 13] have been used to determine catecholamines. Consequently, identifying catecholamines using modified electrodes via distinct electrochemical techniques has been increasing compared with other techniques, because the method does not need any sample pre-treatment and can be conducted in situ. Further, this method is highly sensitive, less time-consuming, and economical [14, 15].

The structures of DA and EP are similar, and these compounds often coexist in biological

* Corresponding Author Email: *kh.ghanbari@alzahra.ac.ir*

samples. Therefore, the simultaneous determination these species is difficult by the electro-oxidation process due to their mutual interference. Thus, developing an effective electrochemical sensor is of significant importance to monitor and determine catecholamines in authentic samples [3].

As a two-dimensional carbon sheet, atoms can refer to graphene, bonded by sp^2 hybridization [16, 17]. Graphene has been widely used in manufacturing devices based on biosensors and sensors due to its high specific surface area, high mechanical strength, high thermal and electrical conductivity, and low cost [18, 19]. For example, Lee et al. made a nano-electrode from gold nanoparticles and graphene sheets coated on a glassy carbon electrode for determining dopamine. There are several methods for preparing graphene, including the reduction of graphene oxide (GO). Techniques such as chemical reduction [20], thermal reduction [21], and electrochemical reduction [22] can be used to reduce graphene. GO reduction is widely used for synthesizing graphene.

Peak current, sensitivity, and reproducibility are improved by preparing a working electrode using nanoparticles. Developing novel electrode surface modifiers is essential in current science and technology [23, 24]. Metal nanoparticles (MNPs) have been extensively used to develop electrochemical sensors by forming novel compounds with different properties. MNPs facilitate the electron transfer process on the surfaces of compounds used in electrocatalysis. Many metal nanoparticles, such as SiO_2, Au, Cr_2O_3, CeO_2, MnO_2, and TiO_2, have been applied to construct biosensors [25-29]. Among them, TiO_2 nanoparticles have attracted considerable interest due to their superior properties, such as their large specific surface area, inexpensiveness, high uniformity, relatively high electrical conductivity, long-term stability, and good biocompatibility [30-32].

Graphene sheets can be used as good support for TiO_2 nanoparticles due to their large surface area and unique electronic properties, leading to increased electrocatalytic activity and attaining a uniform distribution without association. Recent studies have shown that graphene oxide/TiO_2 nanocomposite improves the electrochemical performance by providing a low-resistance charge transfer conduction pathway through the film. These results indicate that GR–TiO_2 film is a suitable electrode material for electrochemical

sensing applications [33].

A chemical method for the synthesis of reduced graphene oxide/TiO_2 nanocomposite modified glassy carbon electrode is reported in this work, which will be used for the simultaneous determination of two catecholamines, dopamine and epinephrine, in real samples. The as-prepared RGO/TiO_2 nanocomposite exhibits significant electrocatalytic activity towards dopamine and epinephrine reduction. These two species can be simultaneously detected on the RGO/TiO_2 nanocomposite modified GCE with high selectivity in a wide linear range. This work presents an easy and efficient method to prepare RGO/TiO_2 nanocomposite for electrochemical sensor applications.

EXPERIMENTAL

Chemical and Reagents

Dopamine (DA) and epinephrine (EP) were purchased from Sigma-Aldrich. Sulfuric acid (H_2SO_4), phosphoric acid (H_3PO_4), acetic acid (HOAC), sodium hydroxide (NaOH), sodium borohydride ($NaBH_4$), titanium dioxide (TiO_2), boric acid (H_3BO_3), and dimethylformamide (DMF) were from Merck. The graphene oxide powder with the purity of 99% was supplied from Nanoscale. All of these materials were analytical grade and used without re-purification. Additionally, all the solutions were prepared with distilled water. Britton–Robinson buffer solution (BRS, 0.04 M, pH 7.0) was employed as a supporting electrolyte, and all the experiments were conducted at room temperature.

Apparatus

A Metrohm Autolab B. V.s Autolab PGSTAT 101 potentiostat/galvanostat (Utrecht, UT, the Netherlands) was used for electrochemical measurements, including CV and DPV. A three-electrode system including a glassy carbon electrode (GCE) with a diameter of 2.5 mm as the working electrode, platinum wire as the counter electrode, and Ag/AgCl as the reference electrode was applied (from the Azar electrode, Urmia, Iran). Field emission scanning electron microscopy (MIRA 3, TESCAN, Czech Republic) was used at 20 kV accelerating voltage to observe the morphology of the studied surfaces. Raman tests by a Thermo Nicolet Dispersive Raman Spectrometer were performed (equipped to a 532 nm Laser beam at 30 mW; a charge-coupled device

detector with a 4 cm^{-1} resolution). X-ray diffraction (XRD) (Model: X'Pert MPD, Company: Philips, Netherlands) was utilized for studying the crystal structure. Xray photoelectron spectroscopy (XPS) was performed using a Gammadata-Scienta ESCA 200 hemispherical analyzer equipped with an Al Ka X-ray source (1486.6 eV) with a monochromator. The binding energies were calibrated based on the C 1s peak at 285 eV.

Preparation of RGO and RGO/TiO$_2$ nanocomposite

The following procedure was implemented for preparing the reduced graphene oxide. First, 100 mg of graphene oxide was mixed with 75 ml of water and placed in an ultrasonic bath for 1 hour. Then, 200 mg of NaBH$_4$ was added to this solution and stirred vigorously for 30 minutes; the solution was then heated at 135 ° C for 6 hours. After that, it was centrifuged, washed with distilled water, dried by heating at 60 ° C for 6 hours, and named RGO [34].

As shown in scheme 1, RGO/TiO$_2$ was synthesized through a two-step method. At first, 0.05 g of RGO and 0.02 g of TiO$_2$ were separately added to ethanol, each followed by ultrasonication for 30 min. Then, RGO and TiO$_2$ solutions were mixed and sonicated for 30 min, followed by half an hour of stirring. After that, the solution was refluxed for 5 hours at 70˚C and centrifuged after cooling. The final product was washed with ethanol, dried by heating at 60 °C for 3 hours, and named RGO/TiO$_2$ nanocomposite.

Fabrication of the modified electrodes

First, the glassy carbon electrode (GCE) was thoroughly polished onto a soft cloth with 0.05 μm alumina powder. Then, the GCE was placed in a solution of distilled water and sulfuric acid at a ratio of 1:10 for 5 minutes in an ultrasonic bath to thoroughly clean the alumina particles on the electrode surface. After that, it was completely washed and utilized in a 0.1 M sulfuric acid solution in a cyclic range of -1.0 to 1.0 V vs. Ag/AgCl to obtain reproducible voltammograms.

0.5 mg of RGO and 0.5 mg of RGO/TiO$_2$ were dissolved separately in 0.5 ml DMF and placed in an ultrasonic bath for 1 hour to open the graphene plates [35, 36]. Then, 8 μL of these solutions were dropped on the surface of the clean bare GCE to modify the surface of the electrode. These modified electrodes were named GCE/RGO and GCE/RGO/TiO$_2$.

RESULTS AND DISCUSSION
Characterization of the RGO/TiO$_2$ nanocomposite

Field emission scanning electron microscopy was used to evaluate the structure, amount, and manner of particle aggregation and average particle size, as well as the presence of amorphous materials in the synthesized nanocomposite. Fig. 1A shows the structure and wrinkle-like morphology of the chemically reduced graphene. Graphene has a
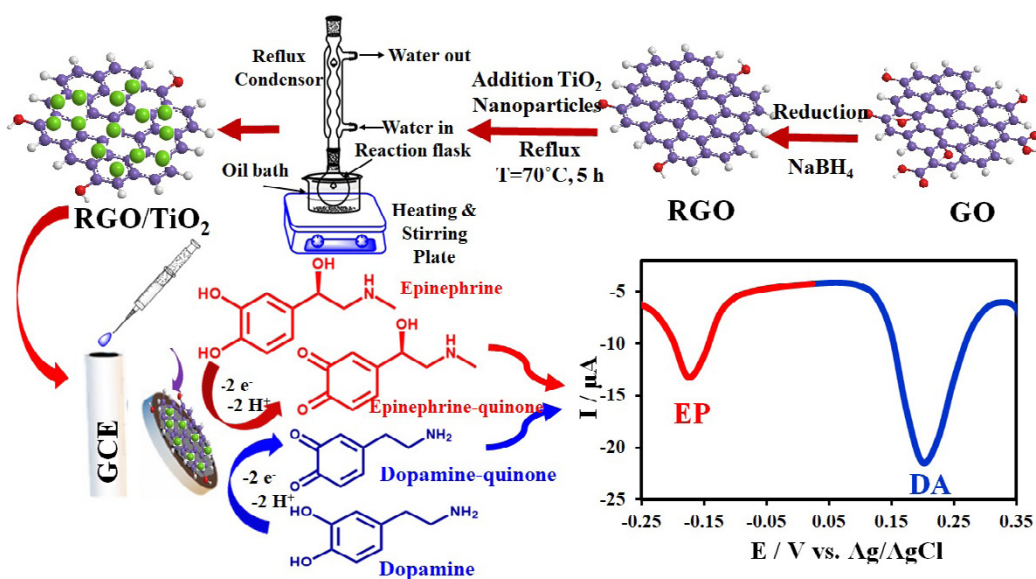
Scheme 1. Schematic illustration of RGO/TiO$_2$ for simultaneous determination of DA and EP.

layered structure that forms intertwined graphene plates which have folds and waves and increase surface conductivity. Fig. 1B indicates the structure of the RGO/TiO$_2$ nanocomposite. Titanium dioxide nanoparticles with a particle size of about 140-180 nm are evenly and compactly dispersed on the graphene plates [37]. As indicated in Fig. 1C, the distribution of particles is homogeneous, within which the graphene nanosheets are hardly visible. Furthermore, the surface of these nanosheets is saturated with TiO$_2$ nanoparticles, which, due to their conductivity, can change the stability and sensitivity of the modified electrode to oxidize and reduce biological molecules.

Energy-dispersive X-ray spectroscopy (EDX)

and elemental mapping spectroscopy were recorded to confirm and investigate the uniform distribution of elements in the RGO/TiO$_2$ nanocomposite structure (Fig. 2(A-E)). The results indicate that the elements carbon (C), oxygen (O), and titanium (Ti) are distributed in the nanocomposite structure.

The FT-IR spectra of GO, RGO, and RGO/TiO$_2$ nanocomposite are shown in Fig. 3. The presence of different types of oxygenated functional groups in the FT-IR spectrum of graphene oxide (curve (A)) confirms the successful oxidation of graphite. The stretching and bending vibrations of the hydroxyl (O-H) groups of water-adsorbed molecules on graphene oxide can be proved by the presence of a wide peak at 3420 cm^{-1}. These polar groups form a
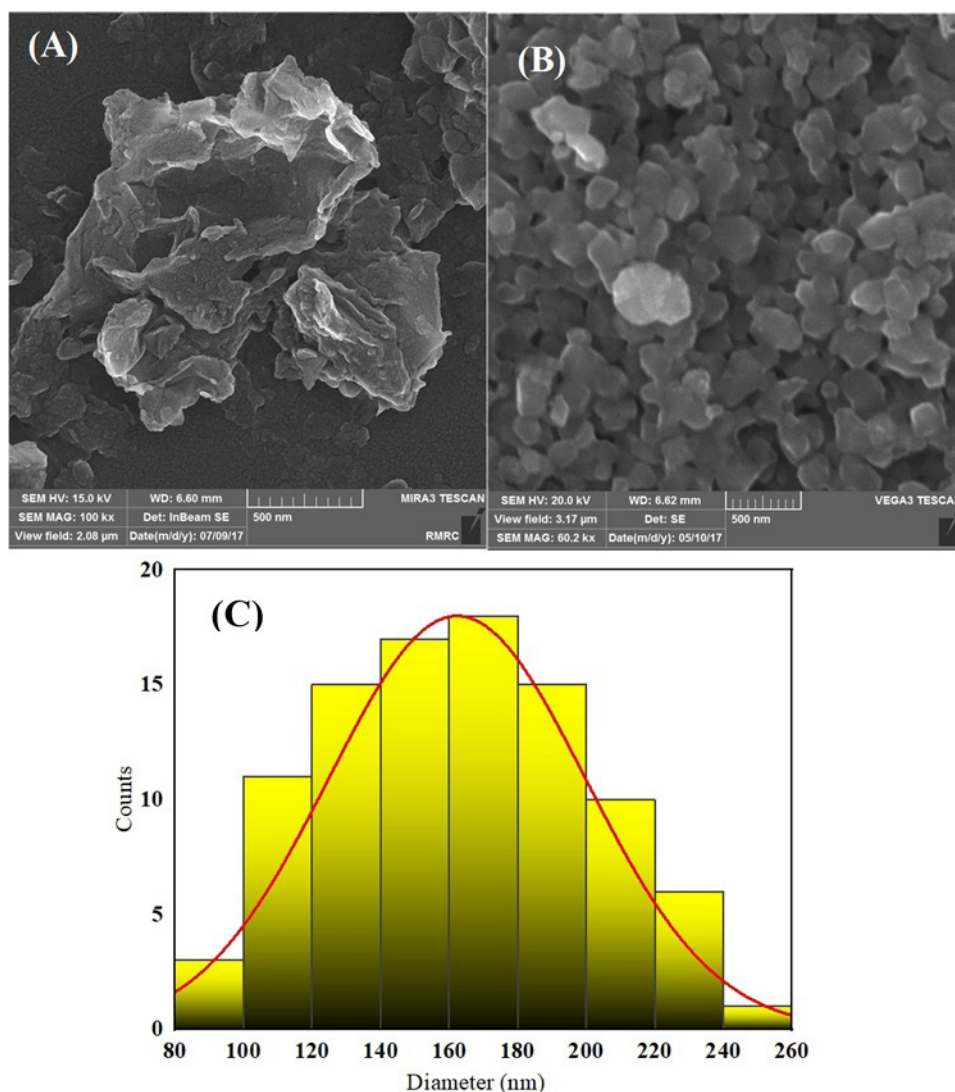

Fig. 1. FE-SEM images of RGO (A) and GO/TiO$_2$ nanocomposite (B), and Histogram was obtained from the Anix Emica software (C).
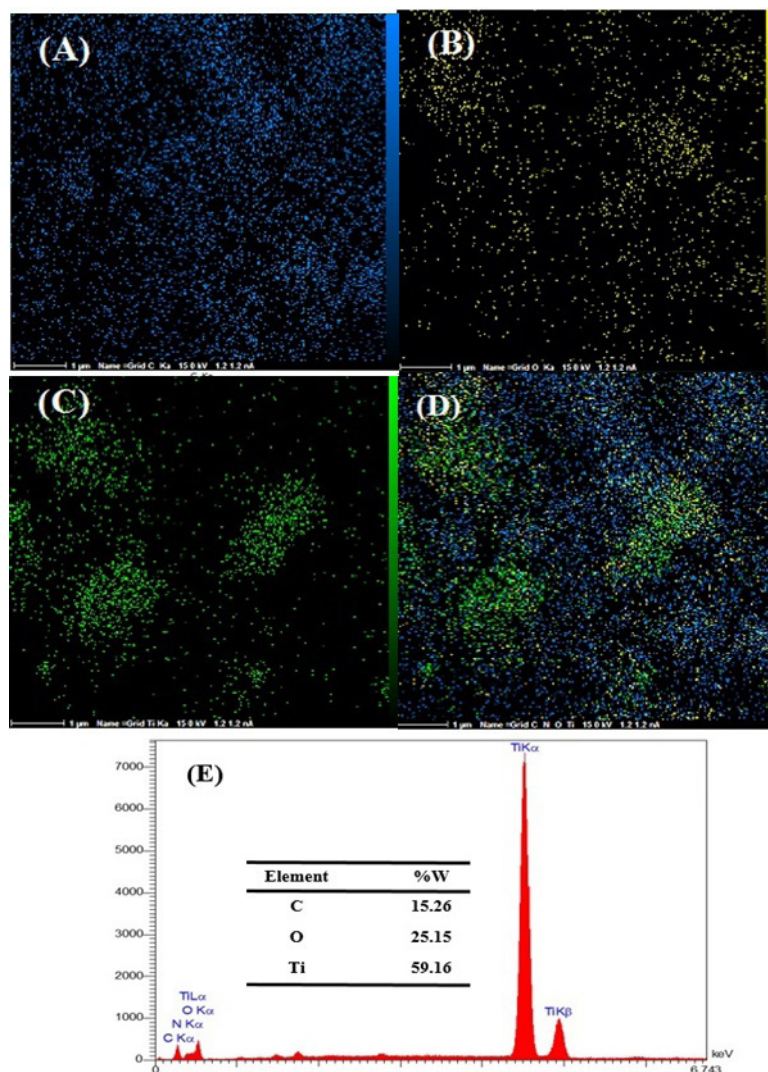
Fig. 2. EDX mapping of C (A), O (B), Ti (C), C, O, and Ti (D) and EDX spectra (E) of RGO/TiO$_2$

hydrogen bond between graphene oxide and water molecules, confirming that the nature of graphene oxide is hydrophilic. The stretching vibrations of the C=C groups in the benzene ring (non-oxidized graphite skeleton vibrations) and the C=O groups of Carboxylic and carbonyl ions present at the edges of graphene oxide appeared in the middle frequency regions, at 1649 and 1699 cm^{-1}, respectively. The two absorption peaks at 1421 and 1458 cm^{-1} are attributed to the C-OH stretching vibrations of the carboxyl groups. Additionally, the sharp peak in 1064 cm^{-1} is consistent with the C-O stretching vibrations of CO$_2$ and alkoxy groups. Finally, the absorption peak at 1170 cm^{-1} is ascribed to the stretching vibrations of the epoxy

groups. The absorption peaks at 2854 and 2925 cm^{-1} demonstrate the symmetric and asymmetric stretching vibrations of CH$_2$. These results confirm that the oxygenated functional groups are present on the surface of graphene oxide [38].

In the FT-TR spectrum of the RGO (curve (B)) the peaks at 1421 and 1458 cm^{-1} belonging to the C-OH stretching vibrations of the carboxyl groups have almost disappeared. Furthermore, the peaks at 1649 and 1170 cm^{-1} are disappeared, which belong to the stretching vibrations of the C=C groups of the benzene ring (vibrations of the non-oxidized graphite skeleton) and epoxy groups, respectively. These results confirm the successful reduction of graphene oxide to graphene.
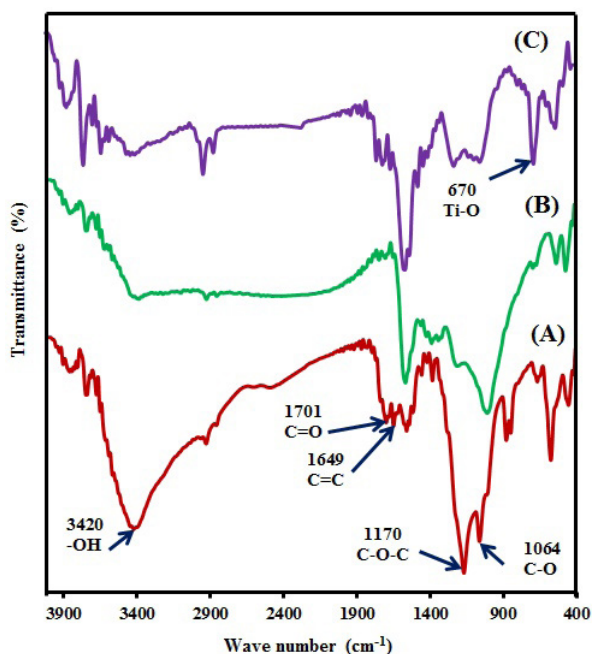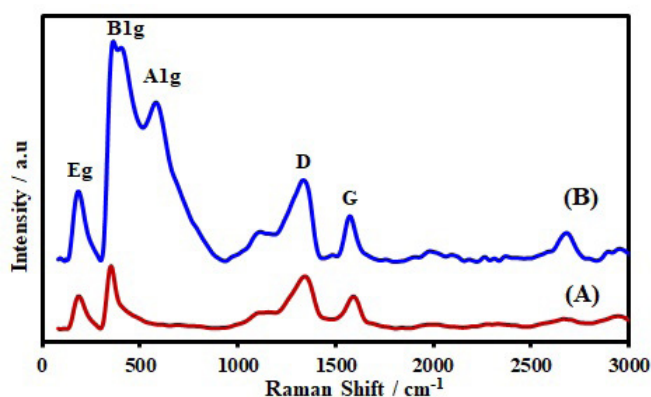
Fig. 3. FT-IR spectra of GO (A), RGO (B), and RGO/TiO$_2$ (C)

Fig. 4. Raman spectra of RGO (A), and RGO/TiO$_2$ (B).

In the FT-IR spectrum of the RGO/TiO$_2$ nanocomposite (curve (C)) shifts are observed in several peaks with the change in peak intensity compared to RGO. Moreover, the presence of a peak at 670 cm^{-1} proved TiO$_2$ presence. All these observations confirm the accuracy of RGO/TiO$_2$ nanocomposite synthesis.

Raman spectroscopy is a helpful technique for surveying the chemical structures of carbon-based materials. Fig. 4 shows the Ramon spectra of RGO and RGO/TiO$_2$ in the range of 0-3000 cm^{-1}. Curve (A) indicates the spectrum of reduced graphene oxide in which two sharp and intense

peaks at 1345 and 1593 cm^{-1} belong to the D and G bands, respectively. The G-band corresponds to the intraplate vibrations of the sp^2 hybrid in carbon chains, and the D-band indicates the sp^3 carbon [38]. The D-to-G bond strength ratio indicates the size of the sp^2 chains and the structural irregularities in the graphene sheets. In the RGO Raman spectrum, the ratio of the D to G band is 1.7.

Curve (B) the Ramon spectrum of RGO/TiO$_2$, demonstrates that the ratio of the D to G band is 1.3, which decreases compared to RGO, indicating an increase in sp^2 chain size and a
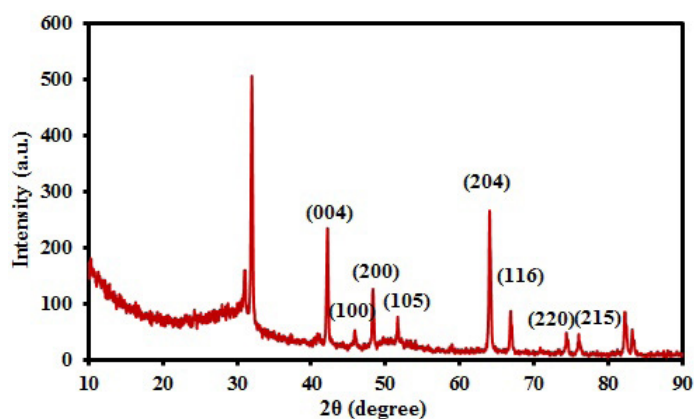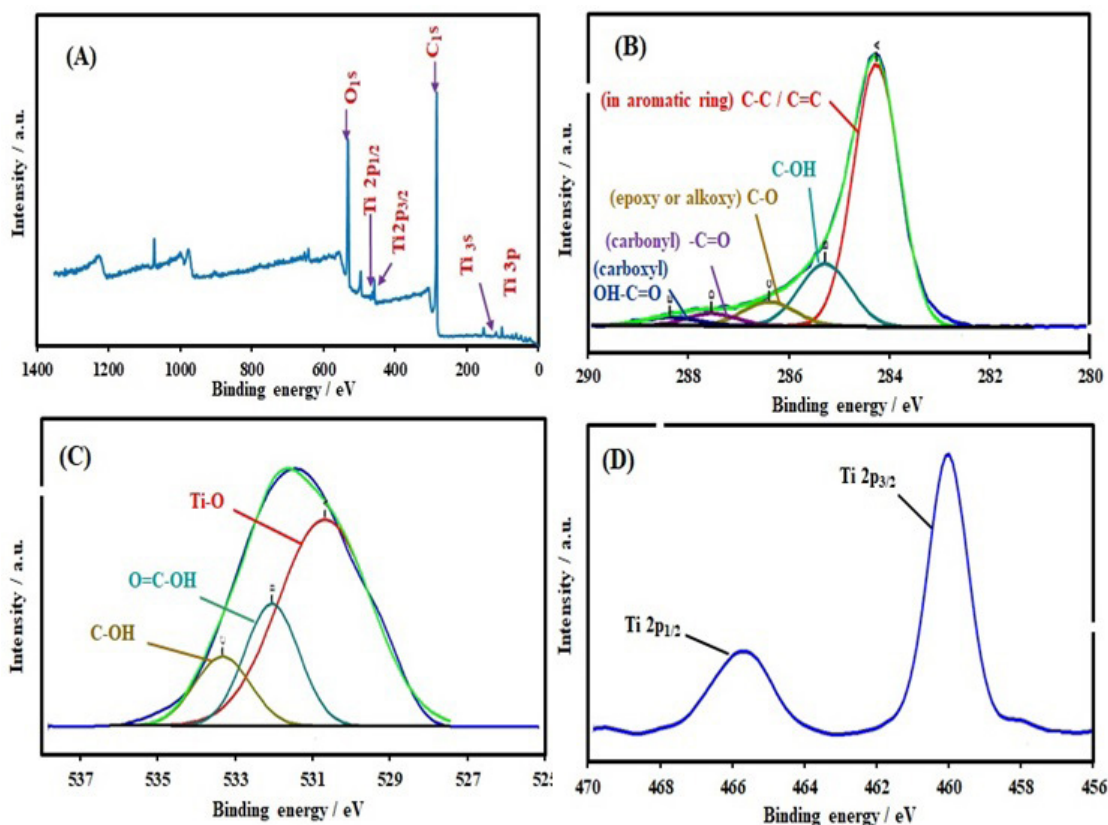
Fig. 5. XRD pattern of the RGO/TiO$_2$

Fig. 6. XPS spectra analysis of RGO/TiO$_2$ nanocomposite (A) Survey, (B) C (1s), (C) O (1s), (D) Ti (2p).

decrease in structural irregularities in reduced graphene oxide. This is a reason for the interaction between the reduced graphene oxide and the titanium dioxide nanoparticles. Further, in RGO/TiO$_2$ nanocomposite, in comparison to RGO, the D and G band have shifted from 1345 to 1337 cm^{-1} and 1593 to 1575 cm^{-1}, respectively. These shifts

towards lower wavenumbers indicate an interaction between reduced RGO and TiO$_2$ nanoparticles [39]. Furthermore, in the RGO/TiO$_2$ Raman spectrum, there are peaks at 205, 424, and 599 cm^{-1}, corresponding to Eg, B1g, and A1g, respectively. These peaks represent the anatase phase structure of TiO$_2$ and the presence of a peak at 2648 cm^{-1},

indicating the presence of RGO as monolayer graphene in the nanocomposite structure [40].

The crystal structure of the nanocomposite was investigated by X-ray diffraction (XRD). Fig. 5 shows the XRD spectrum of the RGO/TiO$_2$ nanocomposite in which the peaks located at 2θ values equal to 42.2°, 45°, 48.3°, 51.6°, 64.0°, 66.9°, 74.4°, 76.0° correspond to the (004), (100), (200), (105), (204), (116), (220), and (215) planes of RGO/TiO$_2$ nanocomposite, respectively [37, 40]. The peak observed at 45.9° is related to the reduced graphene oxide, and the other peaks are attributed to the structure of the TiO$_2$ anatase form. The peaks at 31° and 32° are related to the NaBH$_4$ which was used to reduce the GO to RGO.

XPS is a powerful tool for identifying the states of elements in bulk materials. Fig. 6 shows the XPS spectra of the RGO/TiO$_2$ nanocomposite. Fig. 6A indicates the survey spectrum of RGO/TiO$_2$ nanocomposite and the surface of this sample containing the elements C, O, and Ti. The spectrum C 1s, shown in Fig. 6B, can deconvolve into five types of carbon bonds in the RGO/TiO2 nanocomposite including 284.23 eV (C-C (graphite carbon)), 285.28 eV (C-OH), 286.41 eV (C-O),

287.58 eV (C=O), and 288.42 eV (O-C=O) [41]. These results confirm the presence of carbon in the RGO/TiO$_2$ nanocomposite. The O 1s spectrum (Fig. 6C) can deconvolve into three peaks at 530.76 eV, 532.14 eV, and 533.44 eV, which correspond to Ti-O, HO-C=O, and C-OH, respectively. These results confirm the presence of oxygen in the RGO/TiO$_2$ nanocomposite. Additionally, the peak observed at 530.76 eV can be related to oxygen networks in TiO$_2$ because oxygen in metal oxides usually appears in the range of 530-532 eV. Fig. 6D shows the deconvolved spectrum for Ti 2p with two peaks in the range of 458.02 eV and 463.84 eV, corresponding to 2p$_{3/2}$ and 2p$_{1/2}$, respectively [42].

Electrochemical behavior of DA and EP at the surface of various electrodes

The electrochemical behavior of DA (Fig. 7A), EP (Fig. 7B), and simultaneous detection of DA and EP (Fig. 7C) were investigated on the bare GCE, GCE/RGO, and GCE/RGO/TiO$_2$ in BRS 0.04 M with pH = 7.0 by cyclic voltammetry. DA manifested a pair of redox peaks (ΔEp=310 mV) with the cathodic peak current of -1.45 μA at the bare GCE (Fig. 7A). The CV DA at GCE/
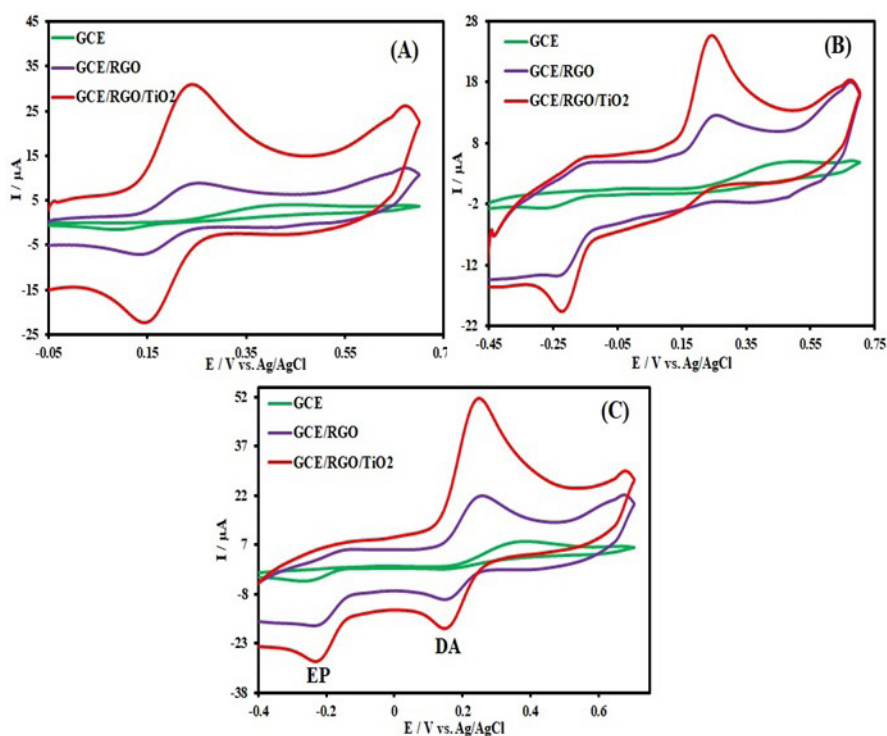

Fig. 7. Cyclic voltammograms of 500 μM DA (A), 500 μM EP (B) and a mixture of 500 μM DA and EP (C) at the surface of a bare GCE, GCE/RGO, and GCE/RGO/TiO$_2$ in 0.04 M BRS solution (pH 7.0) at a scan rate of 100 mVs^{-1}.

RGO and GCE/RGO/TiO$_2$ has two of redox peaks with the potential differences (ΔEp) of 110 mV and 80 mV, respectively. Moreover, the peak intensity significantly increased, which can be attributed to the large specific area of RGO and the electrocatalytic performance of TiO$_2$ nanoparticles. For the GCE/RGO/TiO$_2$, a sharp cathodic peak current of -22.42 µA was observed, approximately 15.5 times larger than the bare GCE. The enhanced electrocatalytic feature may be due to the synergistic effect of RGO and TiO$_2$ nanoparticles.

Similar results for the electrochemical reaction of EP are also observed in Fig. 7B. Only a small cathodic peak of EP was found at the bare GCE while a pair of EP peaks for GCE/RGO and GCE/RGO/TiO$_2$ were observed, the cathodic peak potential of which were -0.228 and -0.218 V, respectively; the peak currents were about -13.80

and -19.63 µA.

The simultaneous detection of DA and EP was also performed (Fig. 7C). At bare GCE, two cathodic peaks for DA (0.144 V) and EP (-0.263 V) with small current intensity were detected. The cathodic peak currents of DA and EP significantly increased for the GCE/RGO and GCE/RGO/TiO$_2$, and the cathodic peak potentials positively shifted. Moreover, two separated reduction peaks were obtained for DA (0.155 V) and EP (-0.233 V); the peak currents were more than 30-fold higher for DA (Ipc = -18.4 µA) and seven-fold higher for EP (Ipc = -28.3 µA) when compared to that of bare GCE. The significant potential separation between DA and EP (0.388 V) allows for the simultaneous determination of DA and EP in mixture samples without interference from the two catecholamines [43]. The composite of RGO and TiO$_2$ with high
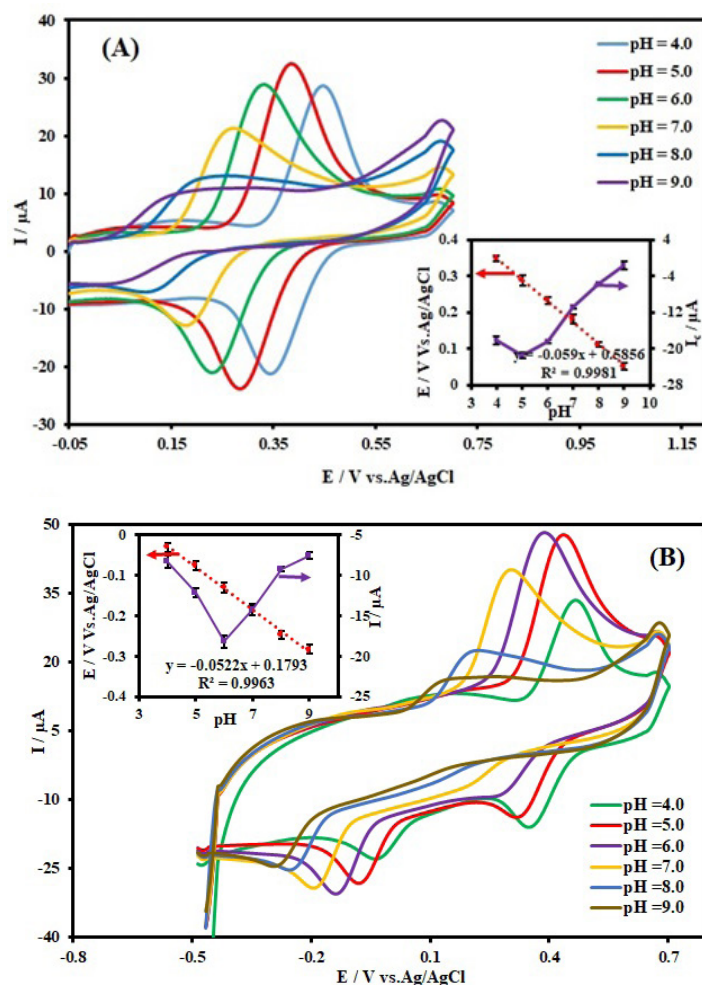

Fig. 8. Cyclic voltammograms of 500 µM DA (A), 500 µM EP (B) at GCE/RGO/TiO$_2$ surface in 0.04 M BRS solution at different pH values (4.0 to 9.0) at a scan rate of 100 mV s^{-1} (Inset: Dependence of peak potential and peak current on pH).

conductivity may offer more active sites and higher surface area, which may be beneficial for electrocatalysis. Moreover, increasing current could be explained by the interaction between the TiO_2 nanoparticles and the –OH groups of DA and EP, leading to an increase in the analyte concentration on the surface of the electrode [44].

Optimization of the experimental conditions

One of the most important and effective parameters in studying the electrochemical behavior of EP and DA is pH. CVs were recorded in a solution of EP and DA at a concentration of 0.5 mM to investigate the pH. As shown in Fig. 8A and B, the maximum currents were observed at the pH of 6.0 and 5.0 for EP and DA, respectively. Further, the potential of both species shifted to a negative value with an increase in pH from 4.0 to 9.0. This negative shift in the potential indicates

that protons are involved in the EP and DA reactions. The reduction peak potential obeys the following equations $Epc = -0.059pH + 0.5856$ ($R^2 = 0.9981$) and $Epc = -0.0522 pH + 0.1793$ ($R^2 = 0.9963$) for DA and EP, receptively. Due to the proximity of the slopes (-0.059 and -0.0522 for DA and EP, respectively) to the theoretical value of -0.059 mV per unit pH, we can conclude that an equal number of electrons and protons were involved in the electrochemical oxidation of EP and DA. Since our goal is to determine of EP and DA at the physiological pH of the body, all the electrochemical tests are performed at the pH of 7.0.

The effect of the scan rate on the electrochemical behavior of 0.5 mM DA and EP in BRS (0.04 M, pH = 7.0) was investigated. Cyclic voltammograms recorded at different scan rates in the range of 20-200 mVs^{-1} at GCE/RGO/TiO_2 surface are shown
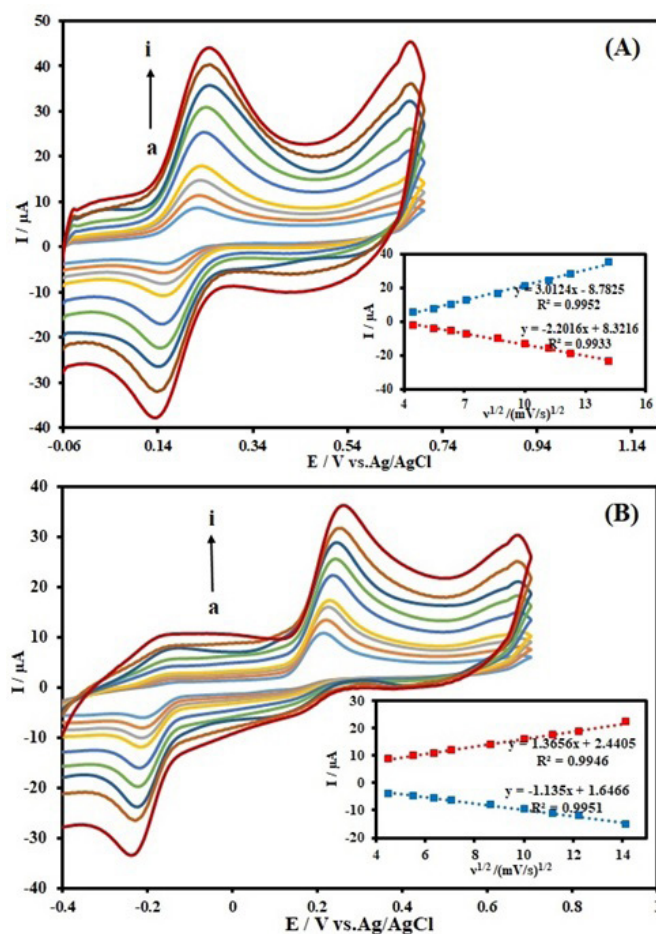

Fig. 9. Cyclic voltammograms of 500 μM DA (A) and 500 μM EP (B) at GCE/RGO/TiO_2 surface in 0.04 M BRS solution at pH 7.0, at various scan rates (a to i; 20-200 mV s^{-1}, respectively). Insets: Plot of I_p vs. $\upsilon^{1/2}$.

in Fig. 9A and B, for DA and EP, respectively. As shown, both currents of anodic and cathodic peaks of DA and EP were enhanced with increasing the scan rate. The linear relationship between the anodic and cathodic peak currents and the squqre root of the scan rate indicates that the electrochemical reactions of both species are under diffusion control, and the GCE/RGO/TiO$_2$ surface is not destroyed by oxidation and reduction of these compounds.

Individual and simultaneous determination of DA and EP

Differential pulse voltammetry (DPV) was conducted to measure DA and EP reduction peaks separately by changing the concentration of each species at the GCE/RGO/TiO$_2$ surface (Fig. 10). DPV curves for the individual detection of DA and EP at GCE/RGO/TiO$_2$ are shown in Fig. 10A

and, respectively. B. As their concentrations rise, their currents increase, and the reduction potential remained constant. As shown in Fig. 10A, there are two linear relationships for DA ranging 3-180 and 180-1000 µM with linear equations calibrated as: I (µA) = -0.0561C$_{DA}$ (µM) – 1.2506, (R^2 = 0.9904) and I (µA) = -0.0026C$_{DA}$ (µM) – 10.408, (R^2 = 0.995). Based on Fig. 10B, the reduction peak currents of EP increases with the increase of EP concentration in the two linear relationships ranging from 4-160 and 160-1000 µM with linear equations calibrated as: I (µA) = -0.0346C$_{EP}$ (µA) – 1.5286, (R^2 = 0.9904) and I (µA) = -0.0044C$_{EP}$ (µA) – 5.8838, (R^2 = 0.9977).

Furthermore, DPV was investigated at GCE/RGO/TiO$_2$ for the simultaneous determination of DA and EP. In a mixture of DA and EP, when the concentration of either DA or EP was changed, the other three (GCE/RGO/TiO$_2$) remained constant.
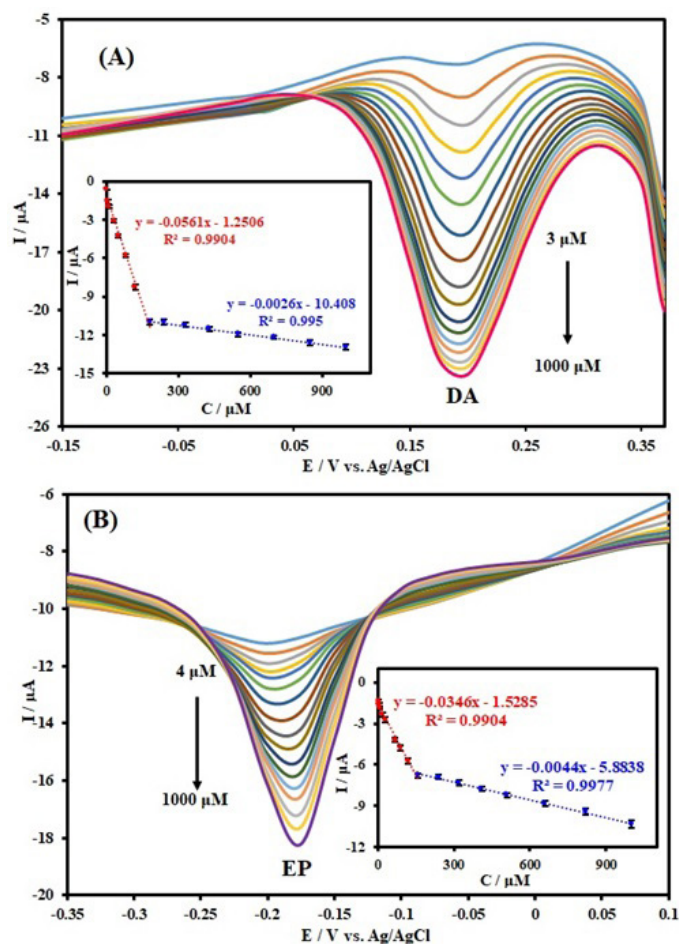

Fig. 10. DPVs of (A) different concentrations of DA (3-1000 µM) and (B) different concentrations of EP (4-1000 µM) at GCE/RGO/TiO$_2$ surface in 0.04 M BRS solution at pH 7.0

As shown in Fig. 11A, the reduction peak currents of DA containing 15 µM EP were enhanced with the increase of the DA concentration and two linear ranges were 3-180 and 180-1000 µM with linear equations calibrated as: I (µA) = -0.048C_{DA} (µM) – 1.6935, (R^2 = 0.9903) and I (µA) = -0.0026C_{DA} (µM) – 9.5644, (R^2 = 0.993). Fig. 11B shows DPV responses for different concentrations of EP in the presence of a fixed concentration of 15 µM

DA. The reduction peak currents of EP increases linearly with the elevation of the EP concentration in two ranges of 5-170 and 170-1000 µM. The linear equations for EP were obtained as: I (µA) = -0.0169C_{EP} (µM) -2.3889, (R^2 = 0.9969) and I (µA) = -0.0051C_{EP} (µM) – 4.5428, (R^2= 0.9915). The detection limits (S/N = 3) for DA and EP were 1.6 and 1.7 µM, respectively.

Fig. 11C shows the DPVs of DA and EP, the
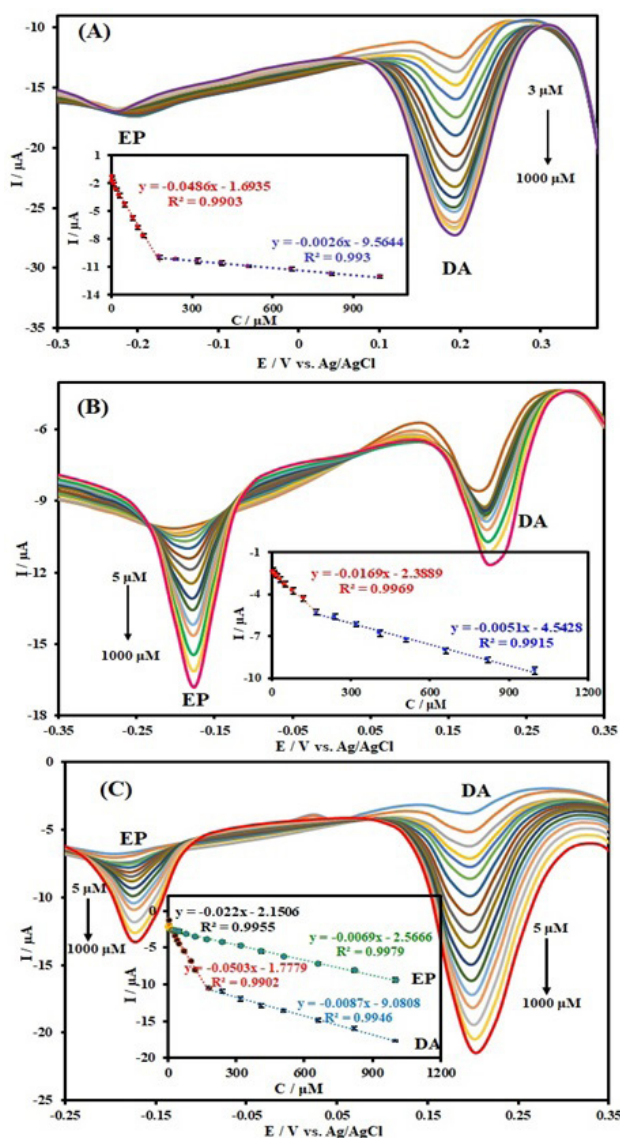
Fig. 11. DPVs of (A) different concentrations of DA (3-1000 µM) in the presence of 15 µM EP; (B) different concentrations of EP (5-1000 µM) in the presence of 15 µM DA, (C) DPV curves for mixtures of DA and EP with different concentrations as follows: (a) 5.0 + 5.0, (b) 7.5 + 7.5, (c) 10 + 10, (c) 15 + 15, (d) 20 + 20, (e) 30 + 30, (f) 50 + 50, (g) 80 + 80, (h) 120 + 120, (i) 180 + 180, (j) 240 + 240, (k) 320 + 320, (l) 410 + 410, (m) 510 + 510, (n) 660 + 660, (o) 820 + 820, and (p) 1000 + 1000 respectively, where the first value is the concentration of DA in µM, and the second value is the concentration of EP in µM, at GCE/RGO/TiO$_2$ surface in 0.04 M BRS solution at pH 7.0, and (Inset: Plots of peak current as a function of the species concentration).

Table 1. Comparison for simultaneous determinations of DA and EP at different modified electrode.

Electrode	Technique	Species	Linear range (μM)	Detection limit (μM)	Ref.
PLA/GCE[a]	DPV	EP	0.5-50	0.1	[45]
		DA	0.8–500	0.3	
AgNPs/SiO$_2$/GO/GCE	DPV	EP	2-80	0.27	[46]
		DA	2-80	0.26	
Poly (DA) nanogold/GCE	DPV	EP	1.0-80.0	0.1	[47]
		DA	1.0-80.0	0.08	
Poly (caffeic acid)/GCE	CV	EP	1.0-35.0	0.2	[48]
		DA	1.0-35.0	0.1	
PAIUCPE[b]	DPV	EP	2.0-150.0	0.327	[49]
		DA	0.8-300.0	0.170	
Poly (taurine)/GCE	DPV	EP	2.0-600.0	0.3	[50]
		DA	1.0-800.0	0.1	
DMSA/Au electrode[c]	CV	EP	10-100	3.5	[51]
		DA	4-90	0.56	
Poly(isonicotinic acid)	CV	EP	5-100	1	[52]
		DA	80-700	20	
Ni$_{3-x}$Te$_2$/CPE[d]	DPV	EP	4-31	0.35	[53]
		DA	4-31	0.15	
Ag-PLC/GCE[e]	CV	EP	5-110	0.8	[54]
		DA	5-110	0.8	
TiO$_2$/RGO/GCE	DPV	EP	5-20 & 20-1000	1.4	This work
		DA	5-180 & 180-1000	1.3	

[a] poly(*L*-arginine)/Glassy Carbon Electrode.
[b] pre-anodized inlaying ultrathin carbon paste electrode
[c] Dimercaptosuccinic acid/gold electrode
[d] Nickel Telluride /Carbon Paste Electrode
[e] Silver-Poly(L-cysteine)/Glassy Carbon Electrode

concentrations of which increased simultaneously in 0.04 M BRS at pH 7.0. The electrochemical responses of the two species increased linearly with their concentrations. The results indicated that the proposed electrode enabled the simultaneous determination of the two species, and the response of peak currents of DA and EP at GCE/RGO/TiO$_2$ were linear with the concentration of each in the ranges of 5-180 and 180-1000 μM for DA and 5-20 and 20-1000 μM for EP. As a result, the linear regression equations for DA and EP were Ip (μ) = -0.0503C$_{DA}$ (μM) – 1.7779 (R^2 = 0.9902), Ip (μ) = -0.0087C$_{DA}$ (μM) – 9.0808 (R^2 = 0.9946), Ip (μA) = -0.022C$_{EP}$ (μM) – 2.1506(R^2 = 0.9955), and Ip (μA) = -0.0069C$_{EP}$ (μM) -2.5666 (R^2 = 0.9979). The limits of detection for DA and EP were 1.3 μM and 1.4 μM (S/N = 3).

The linear dynamic range and detection limit of this sensor with other sensors were compared, and the results are listed in Table 1.

Interference, Reproducibility, and Stability of the electrode
Possible interferences in the detection of DA

and EP at GCE/RGO/TiO$_2$ by adding different species (500 μM of ascorbic acid, uric acid, hypoxanthine, xanthine, tryptophan, lysine, glutamic acid, glucose) to BRS ((0.04 M, pH = 7.0)) in the presence of 10 μM of DA and EP (n=3) were investigated in order to evaluate the selectivity of the proposed method. The tolerance limit, defined as the maximum concentration of the interfering substance, resulted in an error of less than ±5% for determining DA and EP. The results showed that the interferences are only significant at relatively high concentrations, and we can conclude that this sensor is free from common interfering species.

The reproducibility of GCE/RGO/TiO$_2$ was evaluated for the detection of DA, and EP. The standard deviations (RSD) for the five different electrodes produced under the same conditions were 1.20% and 2.30% for DA and EP, respectively, suggesting that GCE/RGO/TiO$_2$ is highly reproducible.

The stability of the fabricated electrode was investigated by storing it in the air at room temperature for two weeks. The peak current maintained at 98.2% for DA and 97.0% for EP from its initial value. These results suggest that the GCE/RGO/TiO$_2$ has good selectivity, reproducibility, and stability.

Table 2. Determination of DA and EP in the pharmaceutical products (n=4) by modified electrode GCE/RGO/TiO$_2$

Sample	Analyte	Added (μM)	Found (μM)	R.S.D (%)	Recovery (%)
Serum 1	DA	0	ND[a]	-	-
		15	13.5	0.8	90.0
		30	29.5	1.1	98.3
	EP	0	-	-	-
		10	9.6	1.0	96.0
		30	30.6	1.3	102.0
Serum 2	DA	0	-	-	-
		50	52.1	1.9	104.2
		75	73.6	1.5	98.1
	EP	0	-	-	-
		60	61.6	2.1	102.7
		100	94.3	0.9	94.3
EP[b]	EP	0	1.92	-	-
		5	4.5	1.5	90.0

[a]Not Detected

[b]Epinephrine ampoule Darou Pakhsh-Iran (1 mg/mL)

Validation of proposed sensor using real samples

GCE/RGO/TiO$_2$ was utilized for determining DA and EP in human blood serum and Epinephrine ampoule (1 mg ml^{-1}) to evaluate the reliability of the method for the analysis of DA and EP in pharmaceutical products. For the purpose, appropriate amounts of diluted samples were transferred into the electrochemical cell using DPV. The analytical results are summarized in Table 2. The recovery ranged from 90.0% to 104.2% for DA and 90.0% to 102.7% for EP; the RSD (n=3) was less than 3.0%. The results are acceptable, demonstrating that the proposed method can be used effectively to determine DA and EP in real samples.

CONCLUSIONS

In this work, we synthesized RGO/TiO$_2$ nanocomposite by a chemical method and used it to modify a GCE. Thus, we built a sensor and used it for the simultaneous determination of EP and DA. The proposed sensor had excellent characteristics such as high levels of sensitivity, selectivity, and reproducibility, and with an acceptable detection limit and linear dynamic range. The structure of the RGO/TiO$_2$ nanocomposite was investigated by FE-SEM, EDX, FTIR, Raman spectroscopy, XRD, and XPS. In addition, the sensor was successfully applied for determining EP, and DA in pharmaceutical formulation samples.

REFERENCES

[1] Banks WA. Enhanced leptin transport across the blood–brain barrier by α1-adrenergic agents. Brain Research. 2001;899(1):209-17.

[2] Goyal RN, Bishnoi S. Simultaneous determination of epinephrine and norepinephrine in human blood plasma and urine samples using nanotubes modified edge plane pyrolytic graphite electrode. Talanta. 2011;84(1):78-83.

[3] Amado J, Gago P, Santos W, Mimoso J, de Jesus I. Cardiogenic shock: Inotropes and vasopressors. Revista Portuguesa de Cardiologia (English Edition). 2016;35(12):681-95.

[4] Colín-Orozco E, Ramírez-Silva MT, Corona-Avendaño S, Romero-Romo M, Palomar-Pardavé M. Electrochemical quantification of dopamine in the presence of ascorbic acid and uric acid using a simple carbon paste electrode modified with SDS micelles at pH 7. Electrochimica Acta. 2012;85:307-13.

[5] Mo J-W, Ogorevc B. Simultaneous Measurement of Dopamine and Ascorbate at Their Physiological Levels Using Voltammetric Microprobe Based on Overoxidized Poly(1,2-phenylenediamine)-Coated Carbon Fiber. Analytical Chemistry. 2001;73(6):1196-202.

[6] Grouzmann E, Tschopp O, Triponez F, Matter M, Bilz S, Brändle M, et al. Catecholamine metabolism in paraganglioma and pheochromocytoma: similar tumors in different sites? PLoS One. 2015;10(5):e0125426.

[7] Liu Y, Zhang J, Xu X, Zhao MK, Andrews AM, Weber SG. Capillary Ultrahigh Performance Liquid Chromatography with Elevated Temperature for Sub-One Minute Separations of Basal Serotonin in Submicroliter Brain Microdialysate Samples. Analytical Chemistry. 2010;82(23):9611-6.

[8] Ji C, Walton J, Su Y, Tella M. Simultaneous determination of plasma epinephrine and norepinephrine using an integrated strategy of a fully automated protein precipitation technique, reductive ethylation labeling and UPLC–MS/MS. Analytica Chimica Acta. 2010;670(1):84-91.

[9] Chung H, Tajiri S, Hyoguchi M, Koyanagi R, Shimura A, Takata F, et al. Analysis of Catecholamines and their Metabolites in Mice Brain by Liquid Chromatography-Mass Spectrometry Using Sulfonated Mixed-Mode Copolymer Column. Analytical Sciences. 2018;18P494.

[10] Nallella PS, Kumar N, Moorkoth S. An Assessment of Crosstalk between Serotonin and Dopamine Systems after Escitalopram Treatment Using LC-MS Technique with Ion-trap Analyser. Indian Journal of Pharmaceutical Sciences. 2020;82(4):612-21.

[11] Ma S, Xu Z, Ren J. Analysis of neurochemicals by capillary electrophoresis in athletes' urine and a pilot study of their changes responding to sport fatigue. Analytical Methods. 2019;11(20):2712-9.

[12] Ghanbari K, Hajian A. Electrochemical characterization of Au/ZnO/PPy/RGO nanocomposite and its application for simultaneous determination of ascorbic acid, epinephrine, and uric acid. Journal of Electroanalytical Chemistry. 2017;801:466-79.

[13] Ghanbari K, Hajheidari N. ZnO–CuxO/polypyrrole nanocomposite modified electrode for simultaneous determination of ascorbic acid, dopamine, and uric acid. Analytical Biochemistry. 2015;473:53-62.

[14] Xiao J, Wang H, Li C, Deng K, Li X. A simple dopamine sensor using graphdiyne nanotubes and shortened carbon nanotubes for enhanced preconcentration and electron transfer. Microchemical Journal. 2021;160:105755.

[15] Veeralingam S, Badhulika S. BiVO4 nanofiber-based field-effect transistors for detection of epinephrine/adrenaline hormones. Materials Chemistry Frontiers. 2021;5(24):8281-9.

[16] Jerome R, Sundramoorthy AK. Preparation of hexagonal boron nitride doped graphene film modified sensor for selective electrochemical detection of nicotine in tobacco sample. Analytica Chimica Acta. 2020;1132:110-20.

[17] Cui F, Zhang X. Electrochemical sensor for epinephrine based on a glassy carbon electrode modified with graphene/gold nanocomposites. Journal of Electroanalytical Chemistry. 2012;669:35-41.

[18] Ghanbari K, Bonyadi S. An electrochemical sensor based on reduced graphene oxide decorated with polypyrrole nanofibers and zinc oxide–copper oxide p–n junction heterostructures for the simultaneous voltammetric determination of ascorbic acid, dopamine, paracetamol, and tryptophan. New Journal of Chemistry. 2018;42(11):8512-23.

[19] Ghanbari K, Ahmadi F. NiO hedgehog-like nanostructures/Au/polyaniline nanofibers/reduced graphene oxide nanocomposite with electrocatalytic activity for non-enzymatic detection of glucose. Analytical Biochemistry. 2017;518:143-53.

[20] Gao X, Jang J, Nagase S. Hydrazine and Thermal Reduction of Graphene Oxide: Reaction Mechanisms, Product Structures, and Reaction Design. The Journal of Physical Chemistry C. 2010;114(2):832-42.

[21] Mutyala S, Mathiyarasu J. A reagentless non-enzymatic hydrogen peroxide sensor presented using electrochemically reduced graphene oxide modified glassy carbon electrode. Materials Science and Engineering: C. 2016;69:398-406.

[22] Ghanbari K, Moloudi M. Flower-like ZnO decorated polyaniline/reduced graphene oxide nanocomposites for simultaneous determination of dopamine and uric acid. Analytical Biochemistry. 2016;512:91-102.

[23] Dashtian K, Hajati S, Ghaedi M. Ti-Based Solid-State Imprinted-Cu$_2$O/CuInSe$_2$ Heterojunction Photoelectrochemical platform for Highly Selective Dopamine Monitoring. Sensors and Actuators B: Chemical. 2021;326:128824.

[24] Ghanbari K, Bonyadi S. An electrochemical sensor based on Pt nanoparticles decorated over-oxidized polypyrrole/reduced graphene oxide nanocomposite for simultaneous determination of two neurotransmitters dopamine and 5-Hydroxy tryptamine in the presence of ascorbic acid. International Journal of Polymer Analysis and Characterization. 2020;25(3):105-25.

[25] Wang Y, Liang Y, Zhang S, Wang T, Zhuang X, Tian C, et al. Enhanced electrochemical sensor based on gold nanoparticles and MoS$_2$ nanoflowers decorated ionic liquid-functionalized graphene for sensitive detection of bisphenol A in environmental water. Microchemical Journal. 2021;161:105769.

[26] Üğe A, Koyuncu Zeybek D, Zeybek B. An electrochemical sensor for sensitive detection of dopamine based on MWCNTs/CeO$_2$-PEDOT composite. Journal of Electroanalytical Chemistry. 2018;813:134-42.

[27] Bavatharani C, Muthusankar E, Alothman ZA, Wabaidur SM, Ponnusamy VK, Ragupathy D. Ultra-high sensitive, selective, non-enzymatic dopamine sensor based on electrochemically active graphene decorated Polydiphenylamine-SiO$_2$ nanohybrid composite. Ceramics International. 2020;46(14):23276-81.

[28] Ghanbari K, Nejabati F. Ternary nanocomposite-based reduced graphene oxide/chitosan/Cr$_2$O$_3$ for the simultaneous determination of dopamine, uric acid, xanthine, and hypoxanthine in fish meat. Analytical Methods. 2020;12(12):1650-61.

[29] Dai Y, Huang J, Zhang H, Liu CC. Highly sensitive electrochemical analysis of tunnel structured MnO2 nanoparticle-based sensors on the oxidation of nitrite. Sensors and Actuators B: Chemical. 2019;281:746-50.

[30] Manjunatha KG, Swamy BEK, Madhuchandra HD, Vishnumurthy KA. Synthesis, characterization and electrochemical studies of titanium oxide nanoparticle modified carbon paste electrode for the determination of paracetamol in presence of adrenaline. Chemical Data Collections. 2021;31:100604.

[31] Li Q, Chen L, Guo C, Liu X, Han D, Wang W. A dual-template defective 3DOMM-TiO2-x for enhanced non-enzymatic electrochemical glucose determination. Journal of Materials Science. 2021;56(4):3414-29.

[32] Veera Manohara Reddy Y, Sravani B, Łuczak T, Mallikarjuna K, Madhavi G. An ultra-sensitive rifampicin electrochemical sensor based on titanium nanoparticles (TiO$_2$) anchored reduced graphene oxide modified glassy carbon electrode. Colloids and Surfaces A: Physicochemical and Engineering Aspects. 2021;608:125533.

[33] Ruiz-Ramirez MM, Silva-Carrillo C, Hinostroza-Mojarro JJ, Rivera-Lugo YY, Valle-Trujillo P, Trujillo-Navarrete B. Electrochemical sensor for determination of nitrobenzene in aqueous solution based on nanostructures of TiO$_2$/GO. Fuel. 2021;283:119326.

[34] Manna B, Retna Raj C. Covalent functionalization and

electrochemical tuning of reduced graphene oxide for the bioelectrocatalytic sensing of serum lactate. Journal of Materials Chemistry B. 2016;4(26):4585-93.

[35] Shehzad N, Tahir M, Johari K, Murugesan T, Hussain M. Improved interfacial bonding of graphene-TiO$_2$ with enhanced photocatalytic reduction of CO$_2$ into solar fuel. Journal of Environmental Chemical Engineering. 2018;6(6):6947-57.

[36] Fan Y, Huang K-J, Niu D-J, Yang C-P, Jing Q-S. TiO$_2$-graphene nanocomposite for electrochemical sensing of adenine and guanine. Electrochimica Acta. 2011;56(12):4685-90.

[37] Liu X, Pan L, Lv T, Zhu G, Lu T, Sun Z, et al. Microwave-assisted synthesis of TiO$_2$-reduced graphene oxide composites for the photocatalytic reduction of Cr(VI). RSC Advances. 2011;1(7):1245-9.

[38] Ghanbari K, Nejabati F. Construction of novel nonenzymatic Xanthine biosensor based on reduced graphene oxide/polypyrrole/CdO nanocomposite for fish meat freshness detection. Journal of Food Measurement and Characterization. 2019;13(2):1411-22.

[39] Zhou K, Zhu Y, Yang X, Jiang X, Li C. Preparation of graphene–TiO2 composites with enhanced photocatalytic activity. New Journal of Chemistry. 2011;35(2):353-9.

[40] Sher Shah MSA, Park AR, Zhang K, Park JH, Yoo PJ. Green Synthesis of Biphasic TiO$_2$–Reduced Graphene Oxide Nanocomposites with Highly Enhanced Photocatalytic Activity. ACS Applied Materials & Interfaces. 2012;4(8):3893-901.

[41] Jin Y-h, Li C-m, Zhang Y-f. Preparation and visible-light driven photocatalytic activity of the rGO/TiO$_2$/BiOI heterostructure for methyl orange degradation. New Carbon Materials. 2020;35(4):394-400.

[42] Li X, Zhao Y, Wang X, Wang J, Gaskov AM, Akbar SA. Reduced graphene oxide (rGO) decorated TiO$_2$ microspheres for selective room-temperature gas sensors. Sensors and Actuators B: Chemical. 2016;230:330-6.

[43] Zhou YZ, Zhang LJ, Chen SL, Dong SY, Zheng XH. Electroanalysis and simultaneous determination of dopamine and epinephrine at poly(isonicotinic acid)-modified carbon paste electrode in the presence of ascorbic acid. Chinese Chemical Letters. 2009;20(2):217-20.

[44] Rastgar S, Shahrokhian S. Nickel hydroxide nanoparticles-reduced graphene oxide nanosheets film: Layer-by-layer electrochemical preparation, characterization and rifampicin sensory application. Talanta. 2014;119:156-63.

[45] Ma W, Sun D-M. Simultaneous Determination of Epinephrine and Dopamine with Poly(L-arginine) Modified Electrode. Chinese Journal of Analytical Chemistry. 2007;35(1):66-70.

[46] Cincotto FH, Canevari TC, Campos AM, Landers R, Machado SAS. Simultaneous determination of epinephrine and dopamine by electrochemical reduction on the hybrid material SiO$_2$/graphene oxide decorated with Ag nanoparticles. Analyst. 2014;139(18):4634-40.

[47] Zhang Y, Ren W, Zhang S. Simultaneous determination of epinephrine, dopamine, ascorbic acid and uric acid by polydopamine-nanogold composites modified electrode. Int J Electrochem Sci. 2013;8(5):6839.

[48] Li NB, Ren W, Luo HQ. Caffeic Acid-Modified Glassy Carbon Electrode for the Simultaneous Determination of Epinephrine and Dopamine. Electroanalysis. 2007;19(14):1496-502.

[49] Huo Je, Li J, Li Q. Study on electrochemical behaviors and the reaction mechanisms of dopamine and epinephrine at the pre-anodized inlaying ultrathin carbon paste electrode with nichrome as a substrate. Materials Science and Engineering: C. 2013;33(1):507-11.

[50] Wang Y, Chen Z-z. A novel poly(taurine) modified glassy carbon electrode for the simultaneous determination of epinephrine and dopamine. Colloids and Surfaces B: Biointerfaces. 2009;74(1):322-7.

[51] Kang WJ, Niu LM, Ma L. 2,3-Dimercaptosuccinic acid self-assembled gold electrode for the simultaneous determination of epinephrine and dopamine. Chinese Chemical Letters. 2009;20(2):221-4.

[52] Zhou YZ, Zhang LJ, Chen SL, Dong SY, Zheng XH, Electroanalysis and simultaneous determination of dopamine and epinephrine. Chinese Chemical Letters, 2009; 20: 217-220.

[53] de Fatima Ulbrich K, Winiarski JP, Jost CL, Maduro de Campos CE. Mechanochemical synthesis of a Ni$_{3-x}$Te$_2$ nanocrystalline composite and its application for simultaneous electrochemical detection of dopamine and adrenaline. Composites Part B: Engineering. 2020;183:107649.

[54] Ma W, Yao X, Sun D. Simultaneous electrochemical determination of dopamine, epinephrine and uric acid at silver doped poly-l-cysteine film electrode. Asian J Chem. 2013;25:6625-34.